CARBON letters

Original Articles
Carbon Letters Vol. 19, 66-71 (2016)

Waste coffee grounds-derived nanoporous carbon nanosheets for supercapacitors

Min Hong Park[1], Young Soo Yun[2], Se Youn Cho[1], Na Rae Kim[1] and Hyoung-Joon Jin[1,♠]

[1]Department of Polymer Science and Engineering, Inha University, Incheon 22212, Korea
[2]Department of Chemical Engineering, Kangwon National University, Samcheok 245-711, Korea

Article Info

Received 5 January 2016
Accepted 25 February 2016

♠Corresponding Author
E-mail: hjjin@inha.ac.kr
Tel: +82-32-860-7483

Open Access

DOI: http://dx.doi.org/10.5714/CL.2016.19.066

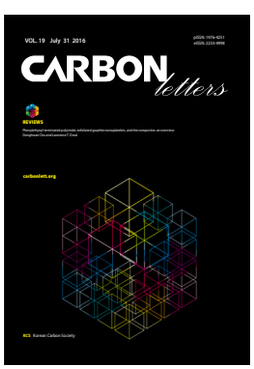

http://carbonlett.org

pISSN: 1976-4251
eISSN: 2233-4998

Abstract

The development of nanostructured functional materials derived from biomass and/or waste is of growing importance for creating sustainable energy-storage systems. In this study, nanoporous carbonaceous materials containing numerous heteroatoms were fabricated from waste coffee grounds using a top-down process via simple heating with KOH. The nanoporous carbon nanosheets exhibited notable material properties such as high specific surface area (1960.1 m^2 g^{-1}), numerous redox-active heteroatoms (16.1 at% oxygen, 2.7 at% nitrogen, and 1.6 at% sulfur), and high aspect ratios (>100). These unique properties led to good electrochemical performance as supercapacitor electrodes. A specific capacitance of ~438.5 F g^{-1} was achieved at a scan rate of 2 mV s^{-1}, and a capacitance of 176 F g^{-1} was maintained at a fast scan rate of 100 mV s^{-1}. Furthermore, cyclic stability was achieved for over 2000 cycles.

Key words: waste coffee grounds, supercapacitor, pyrolysis, carbon nanosheet, nanoporous carbon

1. Introduction

Supercapacitors are energy storage devices that store electrical charge via physical adsorption/desorption processes. These occur between an electrode and electrolyte interface without solid-state-diffusion, leading to high power performance [1]. The electrochemical performance of supercapacitors is highly dependent on the characteristics of the electrode materials used in their fabrication [2,3]. Activated carbon has typically been used as an electrode material due to its high specific surface area, sub-nanometer pores, and high electrical conductivity; in addition to having a low cost of material. However, conventional supercapacitors are limited due to their low energy character. Thus, advanced electrode designs comprising high surface areas, well-defined pore structures, and nano-dimensional structures are required to yield supercapacitors with improved energy and power characteristics [4-7].

Roughly 8 million metric tons of coffee beans are produced and consumed by the global beverage industry each year [8]. For each kilogram of beverage coffee produced, approximately 0.91 kg of waste is generated. Coffee waste is classified as a contaminant because the organic matter in soil consumes large quantities of oxygen while decomposing [9]. Therefore, many studies (spread over various fields) have been performed in search of a method for processing waste coffee grounds (WCGs). WCGs are composed primarily of macromolecular cellulose and lignocellulose, which is known to be an exceptional carbon precursor. The molecular structure of lignocellulose includes aromatic hexagonal carbon atoms that can be carbonized via relatively rapid pyrolysis [10]. Accordingly, the use of WCGs as source for carbon and activated carbon has been widely reported [11-14]. Nevertheless, there are few reports on developing nanostructured carbon-based materials from WCGs.

In this study, nanoporous carbon nanosheets (NCNSs) were fabricated from WCGs via simple heating with KOH. NCNSs were easily obtained through a one-step top-down method from WCGs without any additional treatment. The NCNSs exhibited a high specific surface area of 1960.1 m^2 g^{-1} with numerous redox-active heteroatoms such as oxygen, nitrogen, and sulfur. They also included two-dimensional (2D) nanostructures with high aspect ratios (>100). These superior material properties led to good electrochemical performance as supercapacitor electrodes, exhibiting a specific capacitance of ~438.5 F g^{-1} at a scan rate of 2 mV s^{-1} with good rate capabilities and exceptional cyclic stability.

2. Experimental

2.1. Preparation of carbon materials

The WCGs, from commercial beverage manufacturers (Starbucks®), were dried at 80°C for 48 h. The dried WCGs were mixed at a weight ratio of 1:1 with KOH (95%; Samchun Pure Chemical, Seoul, Korea) in a mortar and were subsequently pyrolyzed in a tube furnace under N_2 gas flow at a heating rate of 10°C min^{-1} up to 800°C, and held at this temperature for 2 h. The resulting NCNSs were washed with deionized water and ethanol to remove leftover residues and then were dried in a vacuum oven at 60°C. For a reference sample, the dried WCGs were pyrolyzed under the same conditions in the absence of KOH. The resultant products are referred to as C-WCGs.

2.2. Characterization

The thermal behavior of the WCGs was analyzed via thermogravimetric analysis (TGA; TG 209 F3, NETZSCH, Germany) from room temperature to 800°C at a heating rate of 10°C min^{-1} under N_2 gas. Samples morphologies were examined via field-emission scanning electron microscopy (S-4300; Hitachi, Tokyo, Japan) and field-emission transmission electron microscopy (JEM2100F; JEOL, Tokyo, Japan). X-ray diffraction (XRD; DMAX2500; Rigaku, Tokyo, Japan) analysis was carried out via Cu Kα radiation (wavelength λ = 0.154 nm) at 40 kV and 100 mA. Raman spectroscopy (Jobin Yvon, Paris, France) was employed to characterize sample microstructures. The chemical composition of the samples was examined via X-ray photoelectron spectroscopy (XPS; PHI 5700 ESCA; Physical Electronics, Chanhassen, MN, USA) with monochromatic Al Kα radiation (hν = 1486.6 eV). The porous properties of the samples were analyzed using nitrogen adsorption/desorption isotherms that were determined using the surface area and a porosimetry analyzer (ASAP 2020; Micromeritics, Norcross, GA, USA) at −196°C. Brunauer-Emmett-Teller (BET) surface areas were calculated according to the BET theory. The micropore surface areas and mesopore surface areas were obtained via t-plot theory and the Barrett-Joyner-Halenda theory, respectively.

2.3. Electrochemical characterization

Electrochemical properties were measured using a three-electrode system consisting of a working electrode (NCNSs), counter electrode (Pt wire), and reference electrode (Ag/AgCl). The NCNSs and polytetrafluoroethylene (60 wt% dispersion in H_2O; Sigma-Aldrich, St. Louis, MO, USA) were mixed in a 9:1 mass ratio and dispersed in ethanol, yielding a homogeneous paste. The ethanol was subsequently evaporated in an oven at 80°C. The resulting mixtures were coated onto nickel mesh (1 × 1 cm). The electrolyte material used was 6 M NaOH and 1 M Na_2SO_4.

3. Results and Discussion

3.1. Thermal decomposition behavior of WCGs

Fig. 1 presents the thermal decomposition behavior of the WCGs. In the first temperature range from ambient to 200°C, a slight weight loss in the TGA curve was attributed to the release of moisture and light volatile materials. The next temperature range from 200°C to 500°C was represented by numerous weight losses (ca. 70%) due to the primary pyrolysis of the WCGs and the formation of carbonaceous materials. In this range of the differential thermogravimetry curve, three peaks were observed that were indicative of the decomposition of hemicellulose, cellulose, and lignin. The last temperature range (to over 500°C) exhibited a slight weight loss resulting from the consolidation of carbon structures [15].

3.2. Morphologies and microstructures of NCNSs and C-WCGs

Morphologies of the carbonaceous materials fabricated from WCGs are presented in Fig. 2. C-WCGs exhibited random micron-scale bulk particle shapes (Fig. 2a and c), while the NCNSs exhibited 2D-like nanosheet structures with high aspect ratios (>100), as shown in Fig. 2b and d. The KOH activation process involved three primary mechanisms according to a prior study [16]: 1) the generation of pore structures via redox reactions between various potassium compounds

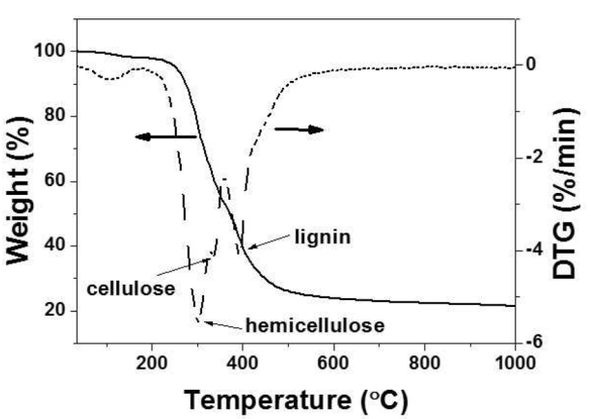

Fig. 1. Thermogravimetric analysis and differential thermogravimetry (DTG) curve of waste coffee grounds.

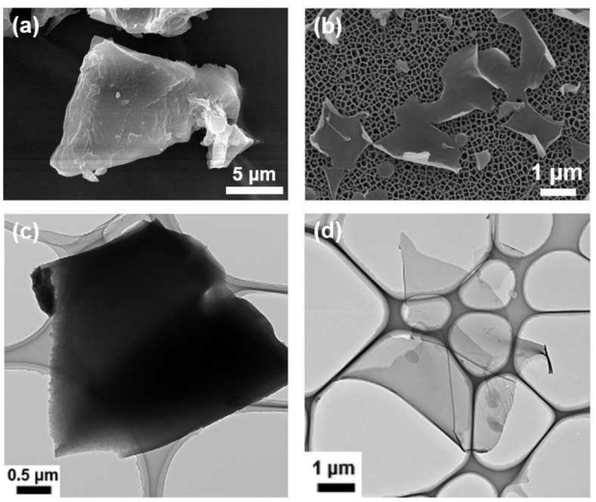

Fig. 2. Scanning electron micrographs of (a) C-WCGs) and (b) nanoporous carbon nanosheets (NCNSs), and transmission electron micrographs of (c) C-WCGs and (d) NCNSs.
C-WCGs : Pyrolyzed WCGs in the absence of KOH

and carbon, 2) the additional development of pore structures via the gasification of carbon, and 3) the expansion of carbon lattices by intercalating metallic K generated during activation into the carbon matrix. Thus, the structural differences between NCNSs and C-WCGs resulted from activation effects in which large quantities of carbon were etched and hexagonal carbon layers were exfoliated via KOH at temperatures above 700°C.

Microstructures of NCNSs and C-WCGs were analyzed via XRD and Raman spectroscopy, as shown in Fig. 3. The XRD pattern of C-WCGs exhibited two broad peaks at 23.3° and 43.3°, corresponding to planar graphite (002), indicating the degree of carbon layer stacking, and (100), indicating the degree of ordered hexagonal carbon structures, respectively (Fig. 3a) [17]. However, the XRD pattern of the NCNSs revealed a very broad graphite (002) peak resulting from carbon layer exfoliation via potassium during the pyrolysis process. By contrast, the Raman spectra of C-WCGs and NCNSs exhibited two distinct peaks centered at 1353 and 1573 cm^{-1}, revealing typical carbon characteristics (Fig. 3b). The *D* band at 1353 cm^{-1} signified a disordered (amorphous) carbon structure, whereas the *G* band at 1573 cm^{-1} was indicative of a hexagonal carbon structure [18]. The integral intensity ratios of the *D* to *G* bands, I_D/I_G, were approximately 1.6 and 2.6, for C-WCGs and NCNSs, respectively. The higher I_D/I_G value of the NCNSs indicated that the NCNSs possessed a greater quantity of defective (amorphous) carbon structures compared to the C-WCGs, which was induced by KOH activation.

3.3. Chemical structure and porous properties of NCNSs

The chemical configuration of NCNSs was characterized via XPS as shown in Fig. 4. In the XPS C 1*s* spectrum, C-O was centered at 285.3 eV and C(O)O was centered at 289.1 eV, with a main C-C bond centered at 284.3 eV. Additionally, C=O and C-O bonds centered at 531.5 and 533.7 eV, respectively, were evident in the O 1*s* spectrum [19]. Nitrogen atoms were present in the form of pyridinic N and pyrrolic N (centered at 398.1 and 400.2 eV, respectively) [20]. In addition, two distinct peaks centered at 164.3 and 168.9 eV were confirmed in the S 2*p* spectrum, indicating that sulfur atoms primarily participated in the formation of C-S and C-SO_x bonds [21]. The heteroatom content of the NCNs was 16.1, 2.7, and 1.6 at% for oxygen, nitrogen, and sulfur, respectively.

The porous properties of the NCNSs were investigated via nitrogen adsorption/desorption isotherm experiments (Fig. 5). The isotherm curves of the NCNSs were representative of International Union of Pure and Applied Chemistry Type-I compounds, indicating the existence of microporous structures (Fig. 5a). The specific surface area of NCNSs was 1960.1 $m^2 g^{-1}$, and most were micropores (1932.5 $m^2 g^{-1}$) ~0.6 nm in size (Fig. 5b). The texture properties of the NCNSs are summarized in Table 1.

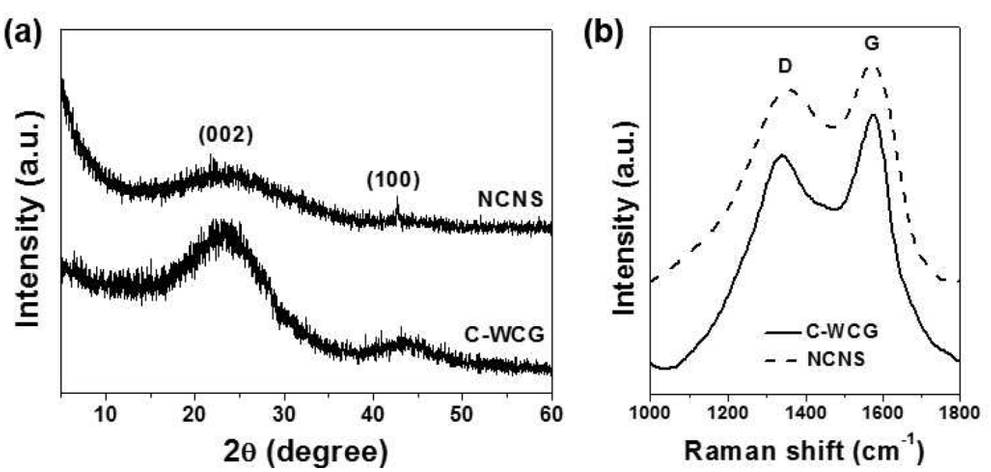

Fig. 3. (a) X-ray diffraction patterns and (b) Raman spectra of C-WCGs and nanoporous carbon nanosheets (NCNSs).
C-WCGs : Pyrolyzed WCGs in the absence of KOH

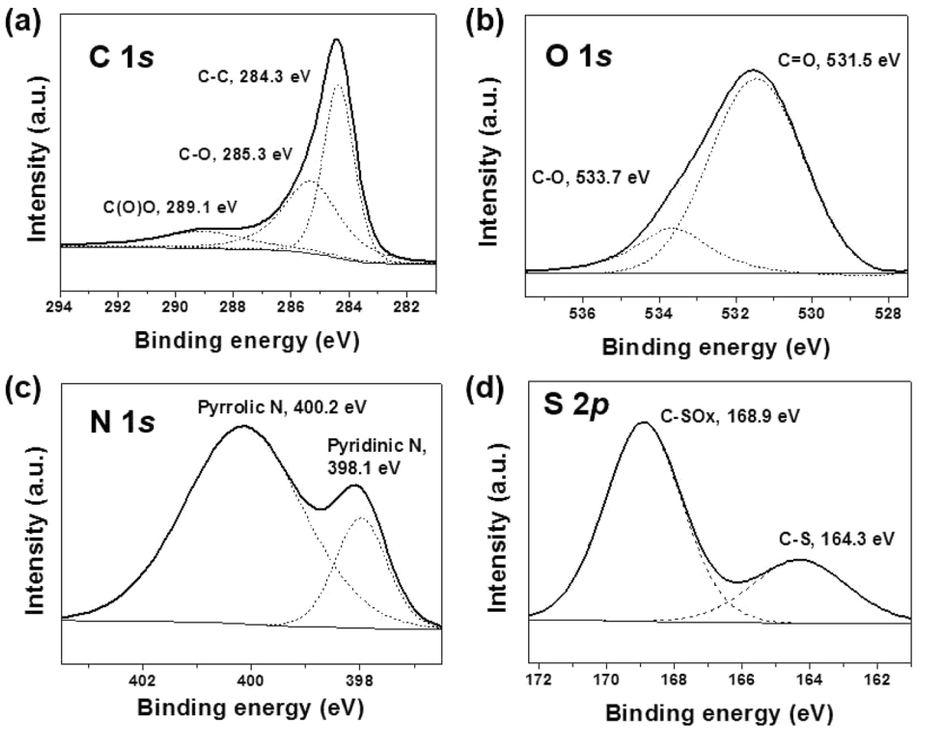

Fig. 4. X-ray photoelectron spectra showing the (a) C 1*s*, (b) O 1*s*, (c) N 1*s*, and (d) S 2*p* of nanoporous carbon nanosheets.

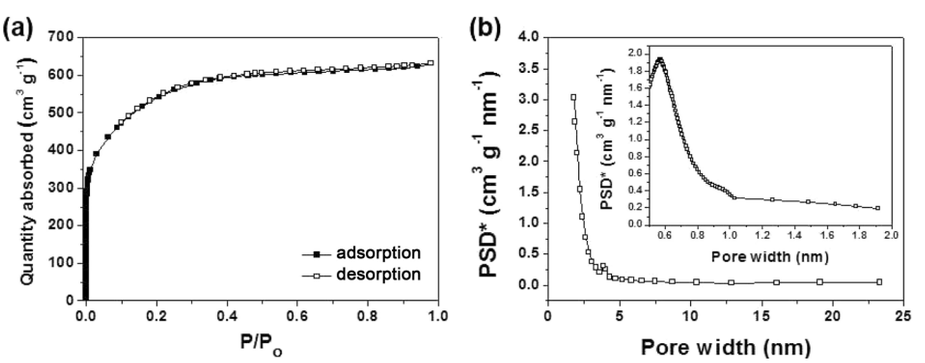

Fig. 5. (a) Nitrogen adsorption/desorption isotherms and (b) mesopore size distribution curves of nanoporous carbon nanosheets (NCNSs). Micropore size distribution curves of NCNSs are shown in the inset.
PSD : Pore size distribution

Table 1. Nanoporous carbon nanosheet textural properties

	S_{BET} (m^2 g^{-1})	S_{micro} (m^2 g^{-1})	S_{meso} (m^2 g^{-1})	D_{micro} (nm)	D_{meso} (nm)
NCNSs	1960.1	1932.5	27.6	0.7	2.3

S_{BET}, Brunauer-Emmett-Teller (BET) surface areas; S_{micro}, micropore surface areas; S_{meso}, mesopore surface areas; D, average pore diameter; D_{micro}, micro pore diameter; D_{mseo}, meso pore diameter, NCNSs, nanoporous carbon nanosheets.

3.4. Electrochemical characteristics of NCNSs

The electrochemical properties of the NCNSs were investigated in aqueous electrolytes (1 M Na_2SO_4 and 6M NaOH) over the potential range between –0.2 and 0.8 (V vs. Ag/AgCl) and –1 and 0 (V vs. Ag/AgCl), respectively. Fig. 6a reveals cyclic voltammogram (CV) curves in 1 M Na_2SO_4 aqueous electrolyte. The CV curves exhibited nearly rectangular shapes, indicating ideal capacitive behavior by the physical adsorption and desorption of sol-

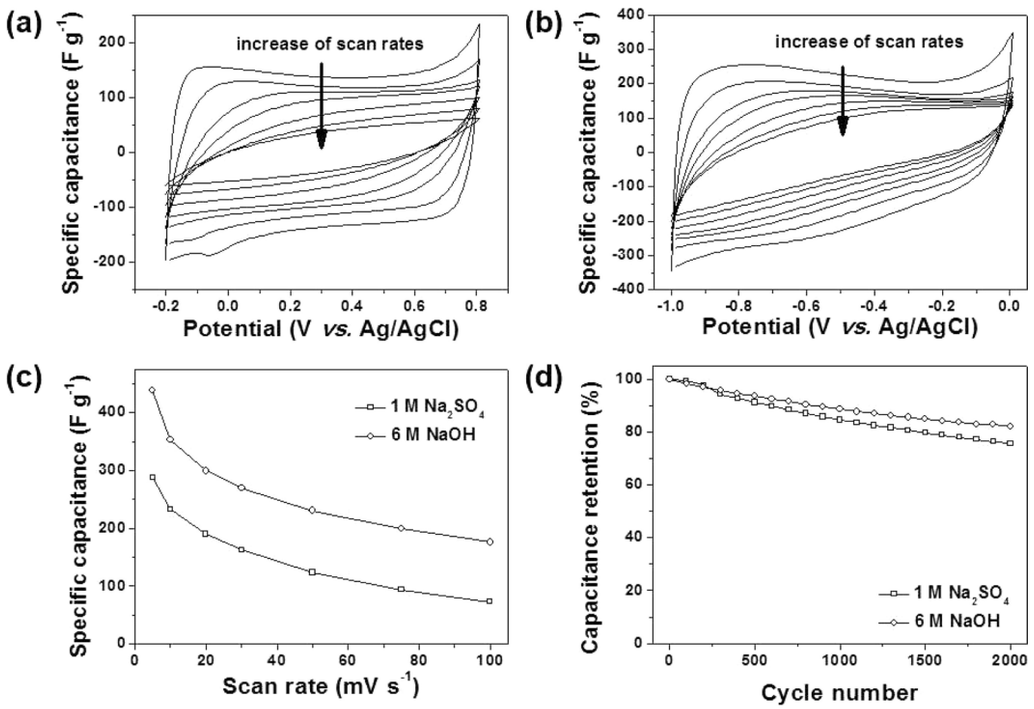

Fig. 6. Cyclic voltammograms of nanoporous carbon nanosheets (NCNSs) in (a) 1 M Na_2SO_4 and (b) 6 M NaOH. (c) Specific capacitance as a function of scan rate and (d) the capacitance retention of NCNSs.

vated anions (hydrated SO_4^-). Steep slopes of the current changes during switching potentials, indicated a small anion-storage mass-transfer resistance. However, with an increase in scan rates, the rectangular CV curves gradually became oval in shape. By contrast, the CV curves in 6 M NaOH aqueous electrolyte exhibited a continual current increase with decrease in the sweeping potential (Fig. 6b). This difference could be induced by pseudocapacitive charges stored in heteroatoms on the surface of the NCNSs [22-24]. In the 6 M NaOH aqueous electrolyte, hydrated Na^+ ions could be charge carriers, in contrast to the 1 M Na_2SO_4 aqueous electrolyte, of which the charge carriers were hydrated SO_4^-. Na^+ could be stored in oxygen, nitrogen, and sulfur atom sites via pseudocapacitive behavior. The specific capacitance of NCNSs in 6 M NaOH was ~438.5 F g^{-1}, which was much higher than the 287.9 F g^{-1} observed for 1 M Na_2SO_4. This capacitance difference supported pseudocapacitance in the 6 M NaOH aqueous electrolyte. Rate performance was investigated at various scan rates (Fig. 6c). As the scan rates were increased, the specific capacitances gradually decreased, and at 100 mV s^{-1}, 176 and 73 F g^{-1} capacitances were achieved in the 6 M NaOH and 1 M Na_2SO_4 aqueous electrolytes, respectively. This indicated good rate performance. Additionally, cyclic stability was maintained over 2000 consecutive cycles (Fig. 6d). After 2000 cycles, NCNSs exhibited capacitance retentions of 81.9% and 75.7% in 6 M NaOH and 1 M Na_2SO_4 aqueous electrolytes, respectively.

4. Conclusions

NCNSs were fabricated from WCGs via simple heating with KOH. The NCNSs exhibited amorphous carbon structures composed of defective hexagonal carbon structures lacking long-range order, as well as high aspect ratios greater than 100. Numerous heteroatoms such as 16.1 at% oxygen, 2.7 at% nitrogen, and 1.6 at% sulfur were confirmed on the surface of the NCNSs, and were present in various chemical structures. Additionally, the NCNSs yielded a high specific surface area of 1960.1 m^2 g^{-1} with a large quantity of sub-nanometer pores. These unique material properties led to good electrochemical performance as supercapacitor electrodes. A specific capacitance of ~438.5 F g^{-1}, good rate capabilities, and stable cyclic lifetimes to over 2000 cycles were achieved with 6 M NaOH aqueous electrolytes.

Conflict of Interest

No potential conflict of interest relevant to this article was reported.

Acknowledgements

This research was supported by Basic Science Research Program through the National Research Foundation of Korea(NRF)

funded by the Ministry of Education (NRF-2016R1A2B4009601 and NRF-2015R1A6A3A01060852). This work also supported by Industrial Strategic Technology Development Program (Project No. 10050477) funded by the Ministry of Trade, Industry & Energy.

References

[1] Simon P, Gogotsi Y. Materials for electrochemical capacitors. Nat mater, **7**, 845 (2008). http://dx.doi.org/10.1038/nmat2297.

[2] Liu C, Li F, Ma LP, Cheng HM. Advanced materials for energy storage. Adv Mater, **22**, E28 (2010). http://dx.doi.org/10.1002/adma.200903328.

[3] Zhang LL, Zhao XS. Carbon-based materials as supercapacitor electrodes. Chem Soc Rev, **38**, 2520 (2009). http://dx.doi.org/10.1039/B813846J.

[4] Aricò AS, Bruce P, Scrosati B, Tarascon JM, van Schalkwijk W. Nanostructured materials for advanced energy conversion and storage devices. Nat mater, **4**, 366 (2005). http://dx.doi.org/10.1038/nmat1368.

[5] Zhu Y, Murali S, Stoller MD, Ganesh KJ, Cai W, Ferreira PJ, Pirkle A, Wallace RM, Cychosz KA, Thommes M, Su D, Stach EA, Ruoff RS. Carbon-based supercapacitors produced by activation of graphene. Science, **332**, 1537 (2011). http://dx.doi.org/10.1126/science.1200770.

[6] Yun YS, Cho SY, Shim J, Kim BH, Chang SJ, Baek SJ, Huh YS, Tak Y, Park YW, Park S, Jin HJ. Microporous carbon nanoplates from regenerated silk proteins for supercapacitors. Adv Mater, **25**, 1993 (2013). http://dx.doi.org/10.1002/adma.201204692.

[7] Yun YS, Cho SY, Kim H, Jin HJ, Kang K. Ultra-thin hollow carbon nanospheres for pseudocapacitive sodium-ion storage. ChemElectroChem, **2**, 359 (2015). http://dx.doi.org/10.1002/celc.201402359.

[8] Jenkins RW, Stageman NE, Fortune CM, Chuck CJ. Effect of the type of bean, processing, and geographical location on the biodiesel produced from waste coffee grounds. Energy Fuels, **28**, 1166 (2014). http://dx.doi.org/10.1021/ef4022976.

[9] Silva MA, Nebra SA, Silva MMJ, Sanchez CG. The use of biomass residues in the Brazilian soluble coffee industry. Biomass Bioenergy, **14**, 457 (1998). http://dx.doi.org/10.1016/S0961-9534(97)10034-4.

[10] Rodríguez-Reinoso F, Molina-Sabio M. Activated carbons from lignocellulosic materials by chemical and/or physical activation: an overview. Carbon, **30**, 1111 (1992). http://dx.doi.org/10.1016/0008-6223(92)90143-K.

[11] Rufford TE, Hulicova-Jurcakova D, Zhu Z, Lu GQ. Nanoporous carbon electrode from waste coffee beans for high performance supercapacitors. Electrochem Commun, **10**, 1594 (2008). http://dx.doi.org/10.1016/j.elecom.2008.08.022.

[12] Rufford TE, Hulicova-Jurcakova D, Fiset E, Zhu Z, Lu GQ. Double-layer capacitance of waste coffee ground activated carbons in an organic electrolyte. Electrochem Commun, **11**, 974 (2009). http://dx.doi.org/10.1016/j.elecom.2009.02.038.

[13] Kante K, Nieto-Delgado C, Rangel-Mendez JR, Bandosz TJ. Spent coffee-based activated carbon: specific surface features and their importance for H_2S separation process. J Hazard Mater, **201-202**, 141 (2012). http://dx.doi.org/10.1016/j.jhazmat.2011.11.053.

[14] Yun YS, Kim DH, Hong SJ, Park MH, Park YW, Kim BH, Jin HJ, Kang, K. Microporous carbon nanosheets with redox-active heteroatoms for pseudocapacitive charge storage. Nanoscale, **7,** 15051 (2015). http://dx.doi.org/10.1039/C5NR04231C.

[15] Sanchez-Silva L, López-González D, Villaseñor J, Sánchez P, Valverde JL. Thermogravimetric–mass spectrometric analysis of lignocellulosic and marine biomass pyrolysis. Bioresour Technol, **109**, 163 (2012). http://dx.doi.org/10.1016/j.biortech.2012.01.001.

[16] Wang J, Kaskel S. KOH activation of carbon-based materials for energy storage. J Mater Chem, **22**, 23710 (2012). http://dx.doi.org/10.1039/C2JM34066F.

[17] Choi YK, Park SJ. Hydrogen storage capacity of highly porous carbons synthesized from biomass-derived aerogels. Carbon Lett, **16**, 127 (2015). http://dx.doi.org/10.5714/CL.2015.16.2.127.

[18] Yun YS, Park MH, Hong SJ, Lee ME, Park YW, Jin HJ. Hierarchically porous carbon nanosheets from waste coffee grounds for supercapacitors. ACS Appl Mater Interfaces, **7**, 3684 (2015). http://dx.doi.org/10.1021/am5081919.

[19] Ganguly A, Sharma S, Papakonstantinou P, Hamilton J. Probing the thermal deoxygenation of graphene oxide using high-resolution in situ X-ray-based spectroscopies. J Phys Chem C, **115**, 17009 (2011). http://dx.doi.org/10.1021/jp203741y.

[20] Yun YS, Im C, Park HH, Hwang I, Tak Y, Jin HJ. Hierarchically porous carbon nanofibers containing numerous heteroatoms for supercapacitors. J Power Sources, **234**, 285 (2013). http://dx.doi.org/10.1016/j.jpowsour.2013.01.169.

[21] Yun YS, Le VD, Kim H, Chang SJ, Baek SJ, Park S, Kim BH, Kim YH, Kang K, Jin HJ. Effects of sulfur doping on graphene-based nanosheets for use as anode materials in lithium-ion batteries. J Power Sources, **262**, 79 (2014). http://dx.doi.org/10.1016/j.jpowsour.2014.03.084.

[22] Andreas HA, Conway BE. Examination of the double-layer capacitance of an high specific-area C-cloth electrode as titrated from acidic to alkaline pHs. Electrochim Acta, **51**, 6510 (2006). http://dx.doi.org/10.1016/j.electacta.2006.04.045.

[23] Hulicova-Jurcakova D, Kodama M, Shiraishi S, Hatori H, Zhu ZH, Lu GQ. Nitrogen-enriched nonporous carbon electrodes with extraordinary supercapacitance. Adv Funct Mater, **19**, 1800 (2009). http://dx.doi.org/10.1002/adfm.200801100.

[24] Zhao X, Zhang Q, Chen CM, Zhang B, Reiche S, Wang A, Zhang T, Schlögl R, Su DS. Aromatic sulfide, sulfoxide, and sulfone mediated mesoporous carbon monolith for use in supercapacitor. Nano Energy, **1**, 624 (2012). http://dx.doi.org/10.1016/j.nanoen.2012.04.003.